Constant-thickness deformation above curved normal faults

ALAN P. MORRIS

Division of Earth and Physical Sciences, University of Texas at San Antonio, TX 78249

and

DAVID A. FERRILL

Center for Nuclear Waste Regulatory Analyses, Southwest Research Institute,
6220 Culebra Road, San Antonio, TX 78238-5166

Abstract—Extensional fault systems are commonly described using models that assume layer-oblique heterogeneous simple shear deformation in fault blocks. These models are colloquially known as vertical or inclined shear models. Less commonly, layer-parallel heterogeneous simple shear is employed; these models are called constant-thickness/flexural-slip models, and have the geometric property that they conserve both bed length and bed thickness. Although popular, vertical or inclined shear models suffer from the limitation that they do not explain two widely observed features of extensional fault systems: crestal collapse grabens, and downwardly blind faults within the hangingwall. Currently used constant-thickness/flexural-slip models are severely limited by their inability to "forward-model" faults with dips (angular bends) greater than 30°. We have modified the most widely used constant-thickness/flexural-slip model so that it can be applied to faults with dips or angular bends greater than 30°. The resulting model can be used to describe the constant-thickness geometry of hangingwalls developed above normal faults of any shape. Alternatively, the model can be used to predict the amount and location of departures from constant-thickness (and constant bed length) deformation in a fault hangingwall, manifest at large-scale by crestal collapse grabens and downwardly blind faults, or at small-scale by sub-seismic resolution faulting.

INTRODUCTION

Normal faults that dip steeply near the surface and less steeply with depth are termed listric. The most common methods for modeling the deformation above listric normal faults rely on heterogeneous simple shear along either vertical or steeply inclined directions within the hangingwall (Verrall, 1981; Groshong, 1989; Dula, 1990; Rowan and Kligfield, 1989). Although these vertical and inclined shear models are widely used and are generally considered to be successful in regions such as the Gulf of Mexico (Rowan and Kligfield, 1989; Xiao and Suppe, 1992), they suffer from the limitation that they do not predict commonly observed large-scale features such as crestal collapse grabens and downwardly blind hangingwall faults.

Classical fault-bend fold theory as codified by Suppe (1983) and widely applied since makes three important assumptions: (1) bedding-normal thickness is preserved during deformation; (2) bed length is preserved during deformation; and (3) there is no net distortion where layers are unbent (no general shear). Constant bed length and thickness are the basic tenets of flexural slip deformation, in which only bent beds have experienced layer-parallel slip, and area is conserved in displacement-parallel cross sections. Assumption (3) requires that there be no "general shear" in the hangingwall fault-bend fold, although Suppe (1983) considers two cases of general shear, one special case for the shearing out of flat-topped folds, and the other more general case of arbitrary hangingwall shear. The no-general-shear constraint limits the strict applicability of Suppe's equations to ramp angles of less than 30°. Consequently, Suppe's (1983) paper and most subsequent treatments have concentrated on contractional deformation in which

the restriction to ramp angles of 30° or less is not a serious limitation because thrust fault ramps commonly dip at such low angles. The principal weakness in the application of flexural slip fault-bend folding to extensional terrains is that normal faults usually dip at angles of 60–70° close to the earth's surface, although fault dip may decrease with depth. Many geologists would prefer to use constant-thickness deformation to model the hangingwalls of listric normal faults to avoid the limitations of vertical and inclined shear models, however the ramp angle restriction has precluded the wide use of constant-thickness fault-bend fold theory in extensional terrains.

It is possible to construct normal-fault trajectories from near-surface data that meet the three assumptions listed above using a modification of the method devised by Geiser *et al.* (1988) for contractional fault-bend folds that have ramps steeper than 30°. Their method involves the restoration of part of the hangingwall onto a known segment of the fault (assumed to have undergone no shape change) and the subsequent reconstruction of this segment in the deformed state using the geometry of a known hangingwall horizon. Several iterations of this procedure will usually produce a listric fault geometry. However, this approach is limited in its use because fault trajectories obtained by this method cannot be forward modeled (i.e., they represent a unique instant in the evolution of the fault for which the assumptions hold). Prior to (less displacement) and following (more displacement) that instant, general hangingwall shear is required for the hangingwall to maintain contact with the fault surface.

In this study, we relax the no-general-shear constraint to allow application of constant-thickness fault-bend fold theory to ramp dips greater than 30°, and to permit the construction of hangingwall geometries above both listric and anti-listric (downward

steepening) normal faults that can be fully forward modeled. Permitting general shear results in multiple solutions for the hangingwall geometry above a curved normal fault. However, incorporation of geological data (constraints on hangingwall deformation) or assumptions of internal deformation (e.g., minimum deformation in the hangingwall) can yield a best-fit solution within a narrow range of possibilities. This approach can account for the formation of large-scale deformation features commonly found in the hangingwalls of normal faults, such as crestal collapse grabens, and downwardly blind faults.

GEOLOGICAL REASONABLENESS

There are two geometrical components to flexural slip deformation of a hangingwall above a curved fault: bending of layers and layer-parallel shear. Extending constant-thickness fault-bend folding to ramp angles or fault bends greater than 30° (see appendix A) requires relaxation of the "no general shear" constraint. Because layer bending and layer-parallel shear can vary once this constraint is relaxed, there is no unique solution for a given fault shape and displacement (Suppe, 1983). It is necessary to choose a set of shear conditions in order to obtain a hangingwall geometry (or specify a hangingwall geometry in order to obtain a set of shear conditions) and this choice is mathematically arbitrary. However, because both bending and shearing of layers require energy, and because the functions describing layer bending and shearing are non-linear, it is possible to define a unique minimum energy (minimum deformation) solution among the large range of potential solutions. Little is known about the energy budget of layer bending and shear, and the details vary from layer to layer within a single lithologic

sequence. However, a best-fit solution can be obtained for a given fault shape and displacement by minimizing first shear and then bending. The "best-fit" solution obtained by our method can be tuned within a narrow range by specifying the rollover dip and predicting layer-parallel shear, or by specifying layer-parallel shear and predicting rollover dip. This provides the geologist with a quantitative means of testing sensitivity to input parameters and assessing the resulting hangingwall deformation.

LISTRIC NORMAL FAULTS

Equation (1) describes the relationship between initial cutoff angle (θ_1), final resting angle (θ_2), bed dip (α), and layer-parallel shear (ψ) for listric faults (see Appendix A for derivation and Fig. 1 for definition of angles):

$$\tan(\psi) = -\cot(\theta_1) + 2\tan\left(\frac{\alpha}{2}\right) + \cot(\alpha + \theta_2) \qquad (1)$$

Because in the general use of this model neither ψ nor α will be known, equation (1) can be graphed. For a pair of θ_1 and θ_2 values, a value of ψ is chosen in the range: $-90° < \psi < 90°$ (negative shear is top away from the fault, positive shear is top towards the fault, during deformation), then α is incrementally varied through the range: $0° < \alpha < 90°$ (overturned beds are not considered). The point at which the difference between the right and left sides of the equation is minimized is found and plotted. This yields four types of ψ versus α curves (Fig. 2). The minimum deformation solution minimizes both shear (ψ) and bending (α). Because negative shear is just as energy consuming as positive shear (negative and positive designation is arbitrary) the preferred natural solution for a θ_1, θ_2

pair will be represented by the nearest approach to zero shear. Curves drawn by solving equation (1) are illustrated in Fig. 5.

Curve Types 1 and 2

Curves exhibiting a single minimum turning point with respect to ψ in the range $0° < \psi < 90°$ are here defined as Type 1 if they have no maximum turning point in this range and Type 2 if they do have a maximum turning point (Figs 2a & b). The rollover dip that corresponds to this minimum turning point is given by (see Appendix A):

$$\alpha_{\psi min} = 60 - \left(\frac{2\theta_2}{3}\right) \qquad (1a)$$

This solution yields minimum deformation solutions where:

$$\cot(\theta_1) < 3\tan\left[30 - \left(\frac{\theta_2}{3}\right)\right] \qquad (1b)$$

Type 2 curves occur where initial cutoff angles (θ_1) are high, and displacements are small (Fig. 2b). They also yield a zero shear solution ($\psi = 0$) but one that corresponds to a high rollover dip. Continued displacement along such faults causes the ψ versus α curve to evolve rapidly to a type 1 (Fig. 3). Therefore the preferred minimum deformation solution corresponds to the lower of the two limb dips (13° with a ψ value of 10°, as opposed to 72° and a ψ value of 0°, in the example given in Figs 2b & 3), which gives a smooth trend for the locus of minimum shear with increasing fault displacement. This is a function of minimizing the combined effects of shear and bending. The energy required

to bend through 13° with a layer-parallel angular shear of 10° is less than the energy required to bend through 72° albeit with zero layer-parallel shear.

Curve Types 3 and 4

Curves that exhibit a single minimum turning point with respect to ψ in the range $-90° < \psi < 0°$ are here defined as Type 3 if they intersect the α-axis once and Type 4 if they intersect the α-axis twice (Figs 2c & d). Type 3 and 4 curves represent the condition:

$$\cot(\theta_1) \geq 3\tan\left[30 - \left(\frac{\theta_2}{3}\right)\right] \qquad (1c)$$

and yield true zero shear solutions. Curves of type 4 have two solutions for which $\psi = 0$ (Fig. 2d). In order to minimize both shear and bending, the shear minimum that corresponds to the lower of the two limb dips is the preferred minimum deformation solution. Solutions to equation (1) for $\theta_1 = 10°$ to 80° and $\theta_2 = 0°$ to 90° in 10° increments are given in the right side of the graphs in Fig. 5.

Interestingly, Fig. 5 illustrates that α value of the minimum turning points of equation (1) depends only on the final resting angle (θ_2), and is independent of cutoff angle (θ_1). This is not true of the ψ value which depends on θ_1. The relationship is illustrated in Fig. 5. The (listric solution) curve for $\theta_2 = 20°$, for example, has a minimum at $\alpha = 47°$ regardless of θ_1. However, the angular shear that corresponds to

this minimum ranges from 48° ($\theta_1 = 80°$) to −23° ($\theta_1 = 30°$), and this corresponding angular shear only represents a minimum deformation solution where equation (1b) holds.

The rules for determining forelimb dip values that correspond to minimum deformation solutions (α_{min}) can be summarized thus:

- If the minimum shear value (ψ_{min}) > 0 then α_{min} is the α value that corresponds to ψ_{min}.
- If (ψ_{min}) < 0 then α_{min} is the α value that corresponds to $\psi = 0$.
- If more than one ψ minima exist, or more than one case where $\psi = 0$, α_{min} is the least α value that corresponds to $\psi = 0$.

ANTI-LISTRIC NORMAL FAULTS

Faults or fault segments that steepen with depth are termed anti-listric. Equation (2) describes the relationship between initial cutoff angle (θ_1), final resting angle (θ_2), bed dip (α), and layer-parallel shear (ψ) for anti-listric faults (Fig. 4). Equation (2) can be graphed in the same way as equation (1). Solutions in the range $-90° < \psi < 90°$ (negative shear is top away from the fault, positive shear is top towards the fault, during deformation), and $0° < \alpha < 90°$ (overturned beds are not considered) yield only one type of curve (Fig. 5) (see Appendix B for derivation):

$$\cot(\theta_1) = \tan(\psi) - \tan\left(\frac{\alpha}{2}\right) + \left[\cot(\theta_1) + \tan\left(\frac{\alpha}{2}\right) - \tan(\psi)\right]^2 \cdot \left[\frac{\sin(\theta_2 - \alpha)\cdot\cos\left(\frac{\alpha}{2}\right)}{\cos\left(\theta_2 - \frac{\alpha}{2}\right)}\right] \qquad (2)$$

Curves drawn by solving equation (2) numerically for $\theta_1 = 10°$ to $80°$ and $\theta_2 = 0°$ to $90°$ in $10°$ increments are given in the left side of the graphs in Fig. 5. All curves have essentially the same form: they are sigmoidal, exhibiting no turning points with respect to ψ, they all yield limb dips synthetic to the dip of the fault (i.e., α is negative in our convention), and all intersect the α-axis (i.e., have zero-shear solutions).

APPLICATIONS

The constant-thickness model presented here extends the range of tools available for the analysis of deformation above curved normal faults. It makes significant contributions to two common problems in cross-section construction and analysis:

(1) The case where the fault trajectory is known or assumed, but the hangingwall geometry is not known; this is the so-called "forward-modeling" scenario.

(2) The case where the fault trajectory is unknown, but the hangingwall geometry is known; this is the so-called "fault trajectory prediction" scenario, or "inverse problem".

Our model also provides new insight in two cases that are not addressed by existing models:

(3) The case where both the fault trajectory and the hangingwall geometry are reasonably well known, but their geometries cannot be explained with internal consistency by an existing deformation model.

(4) The case where the hangingwall contains features such as crestal collapse grabens and/or downwardly tipping normal faults, or is suspected of containing sub-seismic faulting.

Forward-modeling using a minimum deformation approach

It is often convenient and instructive to forward-model hangingwall shapes on a pre-drawn fault shape. We present an algorithm that can be used to perform this task (Appendix C). The values of forelimb dip (α) corresponding to minimum deformation are tabulated in Fig. 6. We treat the hangingwall as a series of initially horizontal segments each of which can be defined in terms of its initial cutoff angle and final resting angle. Once displacement of a horizon along the fault has been specified, the hangingwall geometry can be constructed by obtaining the forelimb dip (from Fig. 6a) and angular shear values (from Fig. 5) consistent with minimum deformation that apply to each hangingwall segment as it rests on the fault. As an example consider a listric normal fault consisting of nine straight-line sections dipping at 80°, 70°, ...0°. In this simple case the vertical separations between fault nodes are constructed to be equal, therefore the hangingwall can be divided into horizontal segments of equal thickness (Fig. 7a). The hangingwall is constructed as a series of angular-bend folds using the appropriate dip domain boundaries. The deformed shape of the hangingwall can be constructed, together with its predicted shear profile (Fig. 7b). Fold geometries can be made more rounded by increasing the angular precision with which the initial fault shape is defined (e.g., 5° increments instead of 10°).

Fault-trajectory prediction using a minimum deformation approach

Using the principle outlined by Geiser *et al.* (1988) it is possible to construct a fault trajectory from a knowledge of the shape of a hangingwall horizon, and the fault trajectory between the footwall and hangingwall cutoffs of this horizon (Fig. 8a). The algorithm presented in Appendix C can be inverted to determine a minimum deformation fault trajectory consistent with the hangingwall geometry. This is possible because the known portion of the fault trajectory constrains the cutoff angle of the hangingwall; and the hangingwall itself provides the forelimb dip angle of the hangingwall segments which can be used to determine the final resting angle (Fig. 8a). The fault trajectory can be sequentially constructed downwards from the lowest known point on the fault (the hangingwall cutoff) by obtaining fault dips that are consistent with the minimum deformation solution represented by the cutoff and final resting angles of each successively deeper hangingwall segment (Figs 8c & 8e). There is some imprecision in this method when obtaining θ_2 values from Fig. 6 because a single forelimb dip (calculated to a precision of 1°) may arise from two final resting angles derived from a single cutoff angle; use of a computer to perform the task can reduce this imprecision.

Strain analysis of cross-sections using non-minimum deformation approach

If sufficient information is available to be confident of both the fault trajectory and the hangingwall fold geometry, and these two are not internally consistent using existing deformation models (vertical or inclined shear, constant-thickness etc.), our model provides a further alternative for analysis (Appendix D). The hangingwall can be divided into segments defined by the initial cutoff angles and final resting angles. Then

using the cutoff angle, final resting angle pair, and Fig. 5, the angular shear for each hangingwall segment can be determined. For example, a hangingwall segment cut from a fault section dipping at 60° ($\theta_1 = 60°$) and resting on a fault section dipping at 20° ($\theta_2 = 20°$) with a forelimb dip angle (α) of 10° does not represent a minimum-deformation solution (forelimb dip angle would be 47°) but should exhibit angular shear (Ψ) of 54°. Once the shear angles for all segments have been determined, the shear profile for the hangingwall can be constructed.

Layer thinning and extension using non-minimum deformation approach

The shear profile described above and Appendix D *may* represent the true state of strain of the sheared layers high in the hangingwall. Alternatively, if the shear strain has not developed in the hangingwall, layers high in the hangingwall must have thinned and/or extended in order to accommodate the required hangingwall strain (Ferrill and Morris, 1997). The model provides a means for quantifying this extension, and therefore predicting the amount of extension accommodated at large-scale by crestal collapse grabens and downwardly blind faults, or at small-scale by more pervasive means such as sub-seismic-resolution faulting.

ALTERNATIVE HANGINGWALL DEFORMATION MECHANISMS

Significance for section restoration and validation

Cross sections constructed for listric normal faults with near-surface dips of 80° using equation (1) and minimizing first shear and secondly bending exhibit two salient features. Beds low in the hangingwall, cut from ramps dipping at 30° or less, can

accommodate bending without accompanying general shear or thickness change (Fig. 9). Beds high in the hangingwall, cut from ramps dipping at higher angles, must undergo either bed-parallel shear or bed-parallel extension in order to maintain constant-thickness (Fig. 9). The method(s) by which the hangingwall accommodates strain in its higher portion is of great interest and our model provides a quantitative means for assessing how that strain is partitioned. Possible mechanisms for hangingwall strain accommodation are: large-scale crestal-collapse grabens and downwardly blind faults (both synthetic and antithetic), and small-scale extensional faults, fractures, and distributed ductile deformation (Ferrill and Morris, 1997). None of the inclined or vertical shear models commonly used to construct and restore extensional fault geometries (Dula, 1990) can explain the common occurrence of large-scale features such as crestal collapse grabens or downwardly blind faults in the hangingwalls of listric normal faults.

Faulting and fracturing

Outer-arc extension in the hangingwall of a listric normal fault is predicted in the model by the shear profile. As quantified here, faulting and fracturing in the hangingwall to accommodate this extension is likely to die out with depth because the necessity for extension decreases with depth. This observation is consistent with the common occurrence of deformation patterns in extensional rollover structures such as crestal grabens and downwardly tipping faults that indicate downward decrease in layer-parallel extension. In addition, by matching the bending of hangingwall beds with the extension that should be associated with that bending, and then comparing this with the actual extension generated by hangingwall faulting, it should be possible to predict how much,

if any, extension has been partitioned into the apparently unfaulted rock mass in the form of smaller-scale extensional faults and fractures. This is of particular interest in areas of petroleum exploration where extension produced by features resolvable on seismic sections could be compared with predicted extension and an estimate of smaller scale features could be made based on the mismatch.

Penetrative shear

In regions where temperature and/or pressure conditions are high during faulting, or where sequences contain weak layers, hangingwall rocks may deform by more ductile mechanisms and penetrative layer-parallel shear may accommodate hangingwall strain. Accumulation of ductile strain in the hangingwall of a brittle fault can occur. Displacement along the fault results in high strain rates within the fault zone, thus promoting brittle behavior even at elevated temperatures and pressures (Ferrill *et al.*, 1998), whereas strains distributed through the hangingwall for a given slip increment accumulate at much slower rates and therefore may be accomplished by more ductile mechanisms (e.g., crystal plastic deformation, grain boundary sliding).

SUMMARY

The constant-thickness deformation model implies flexural shear deformation within fault blocks, but can also be used to predict fault block deformation by other mechanisms. Flexural slip is likely an important deformation mechanism wherever a strong mechanical contrasts exist between rock layers. Such contrasts exist in sedimentary sequences where sand and overpressured shale or evaporites occur, and even

in volcanic rocks where bedded tuffs are inter-layered with welded cooling units. Our approach provides a means for describing these structures that explains such common large-scale features as crestal collapse grabens and downwardly blind faults, and can predict the likelihood and degree of development of small-scale extensional features in the hangingwalls of curved faults.

Acknowledgments—This work was performed at the Center for Nuclear Waste Regulatory Analyses (CNWRA) for the U.S. Nuclear Regulatory Commission (NRC) under contract NRC-02-93-005. This paper is an independent product of the CNWRA and does not necessarily reflect the views or regulatory position of the NRC. We thank Darrell Sims for his critical review and Drs. Budhi Sagar, Lee Abramson, and Pat Nash for their insightful comments on the mathematics of this work. Constructive reviews by Drs. Peter Geiser, Peter Hudleston, and Mark Rowan greatly improved the paper. Annette Mandujano painstakingly produced the final manuscript.

REFERENCES

Dula, W.F., Jr. (1990) Geometric models of listric normal faults and rollover folds. *American Association of Petroleum Geologists Bulletin* **75**, 1609–1625.

Ferrill, D.A. and Morris, A.P. (1997) Geometric considerations of deformation above curved normal faults and salt evacuation surfaces. *The Leading Edge* **16**, 1129–1133

Ferrill, D.A., Morris, A.P., Jones, M., and Stamatakos, J. (1998) Extensional layer-parallel shear and normal faulting. *Journal of Structural Geology* **20,** 355–362.

Geiser, J., Geiser, P.A., Kligfield, R., Ratliff, R., and Rowan, M. (1988) New applications of computer-based section construction: strain-analysis, local balancing, and subsurface fault prediction. *The Mountain Geologist* **25,** 47–59.

Groshong, R. H., Jr. (1989) Half-graben structures: balanced models of extensional fault-bend folds. *Bulletin of the Geological Society of America* **101,** 96–105.

Rowan, M. G., and Kligfield, R. (1989) Cross section restoration and balancing as aids to seismic interpretation in extensional terranes. *American Association of Petroleum Geologists Bulletin* **73,** 955–966.

Suppe, J. (1983) Geometry and kinematics of fault-bend folding. *American Journal of Science* **283,** 684–721.

Suppe, J. (1985) *Principles of Structural Geology.* Prentice-Hall, New Jersey.

Verrall, P. (1981) Structural interpretation with application to North Sea problems. Joint Association of Petroleum Exploration Courses (JAPEC), London, Course Notes No. **3.**

Xiao, H. and Suppe, J. (1992) Origin of Rollover. *The American Association of Petroleum Geologists Bulletin* **76,** 509–529.

APPENDIX A

Fault-bend fold theory extended: listric faults

Fig. 1a illustrates an undeformed, horizontal bed resting against a segmented listric fault surface, figure 1b illustrates the same bed after fault slip such that the whole of the bed has slipped past the fault bend.

Define lengths, assuming conservation of bed length:

$$BE = CD = t$$

$$AB = \frac{t}{\tan(\theta_1)}$$

$$AC = l_o$$

$$A'F = A'I = l_a$$

Line E'F must bisect angle A'FG as a consequence of the requirement of constant bed thickness (e.g., Suppe, 1985, page 63, Fig. 2-24), and defining angles in all the triangles within this angular bend fold gives the equality: $A'FI = A'IF$.

$$FG = l_b$$

$$GC' = l_c$$

$$D'H = t \cdot \tan(\psi)$$

Conservation of bed length requires that:

$$l_0 = l_a + l_b + l_c$$

and that:

$$l_0 - \frac{t}{\tan(\theta_1)} = l_c + t \cdot \tan(\psi)$$

therefore:

$$l_c = l_0 - \frac{t}{\tan(\theta_1)} - t \cdot \tan(\psi)$$

Define angles

$$A'FG = 180 - \alpha$$

$$A'FI = A'IF = \frac{180 - \alpha}{2} = \left(90 - \frac{\alpha}{2}\right)$$

$$FE'G = \frac{\alpha}{2}$$

$$IE'A' = 90 - \frac{\alpha}{2} - \theta_2$$

$$FA'I = \alpha$$

From triangle A'FE' the sine rule gives:

$$\frac{l_a}{\sin\left(90 - \frac{\alpha}{2} - \theta_2\right)} = \frac{FE'}{\sin(\alpha + \theta_2)}$$

From triangle FGE':

$$FE' = \frac{t}{\cos\left(\frac{\alpha}{2}\right)}$$

Therefore:

$$l_a = \frac{t \cdot \sin\left(90 - \frac{\alpha}{2} - \theta_2\right)}{\cos\left(\frac{\alpha}{2}\right) \cdot \sin(\alpha + \theta_2)}$$

From triangle A′IE′ the sine rule gives:

$$\frac{l_a}{\sin\left(90 - \frac{\alpha}{2} - \theta_2\right)} = \frac{A'E'}{\sin\left(90 + \frac{\alpha}{2}\right)}$$

Therefore:

$$A'E' = \frac{l_a \cdot \sin\left(90 + \frac{\alpha}{2}\right)}{\sin\left(90 - \frac{\alpha}{2} - \theta_2\right)}$$

Undeformed area:

$$Area = \left(l_0 - \frac{t}{\tan(\theta_1)}\right) \cdot t + \frac{t^2}{2 \cdot \tan(\theta_1)}$$

Deformed area:

$$AreaA'FI = \frac{l_a^2 \cdot \sin(\alpha)}{2}$$

$$AreaA'IE' = \frac{l_a^2 \cdot \sin(\theta_2) \cdot \sin\left(90 + \frac{\alpha}{2}\right)}{2 \cdot \sin\left(90 - \frac{\alpha}{2} - \theta_2\right)}$$

$$AreaFGE' = \frac{t^2 \cdot \tan\left(\frac{\alpha}{2}\right)}{2}$$

$$AreaC'D'H = \frac{t^2 \cdot \tan(\psi)}{2}$$

$$AreaGC'HE' = (l_c) \cdot t$$

Equate undeformed and deformed areas, substitute for l_a and eliminate t, then substitute for l_c and eliminate l_0, and simplifying gives equation (1):

$$\tan(\psi) = -\cot(\theta_1) + 2\tan\left(\frac{\alpha}{2}\right) + \cot(\alpha + \theta_2) \qquad (1)$$

This equation can be solved numerically by fixing values for θ_1, θ_2, and varying α and ψ.

The minimum turning point of equation (1) can be found by setting:

$$\frac{d(\tan\psi)}{d\alpha} = 0$$

because $\tan(\psi)$ is an increasing function of ψ in the range $-90° < \psi < 90°$.

Thus:

$$\frac{d\left[2\tan\left(\frac{\alpha}{2}\right)\right]}{d\alpha} = -\frac{d\left[\cot(\alpha + \theta_2)\right]}{d\alpha}$$

Using the relationships:

$$\frac{d[\tan(u)]}{du} = \frac{\pi}{90}\left[\frac{1}{\cos^2(u)}\right]$$

and

$$\frac{d[\cot(u)]}{du} = -\frac{\pi}{90}\left[\frac{1}{\sin^2(u)}\right]$$

(for u in degrees).

Therefore:

$$\cos^2\left(\frac{\alpha}{2}\right) = \sin^2(\alpha + \theta_2) \qquad \text{(i)}$$

In equation (i) and for $0 \le \alpha \le (\alpha + \theta_2) \le 180$, both $\cos(\alpha/2)$ and $\sin(\alpha + \theta_2)$ are positive. Therefore we can take the square root of both sides:

$$\cos\left(\frac{\alpha}{2}\right) = \sin(\alpha + \theta_2) \qquad \text{(ii)}$$

Equation (ii) has two solutions depending on whether $(\alpha + \theta_2) \le 90$ or $(\alpha + \theta_2) > 90$.

If $(\alpha + \theta_2) \le 90$ then for all α:

$$\cos\left(\frac{\alpha}{2}\right) = \sin\left(90 - \frac{\alpha}{2}\right)$$

Therefore:

$$\sin(\alpha + \theta_2) = \sin\left(90 - \frac{\alpha}{2}\right)$$

Because both $(\alpha + \theta_2)$ and $(90 - \alpha/2)$ are less than or equal to 90° we can equate them:

$$(\alpha + \theta_2) = \left(90 - \frac{\alpha}{2}\right)$$

Thus the limb dip value for this turning point is:

$$\alpha_1 = 60 - \frac{2\theta_2}{3} \qquad (1a)$$

For the second turning point, we have $(\alpha + \theta_2) > 90$, therefore:

$$\sin(\alpha + \theta_2) = \sin(180 - \alpha - \theta_2)$$

substituting into equation (ii) gives:

$$\cos\left(\frac{\alpha}{2}\right) = \sin\left(90 - \frac{\alpha}{2}\right) = \sin(180 - \alpha - \theta_2)$$

Because the arguments of the sine function are all less than 90°, we can equate them, and the limb dip value for this turning point is:

$$\alpha_2 = 180 - 2\theta_2 = 3\alpha_1$$

From Fig. 5 we see that for listric faults $0 < \alpha < 90$, therefore α_1 corresponds to the minimum turning point.

To obtain conditions for zero shear, first refer to Fig. 2. In order for there to be a zero-shear solution for a given θ_1, θ_2 pair, the minimum turning point of the α versus ψ curve must have a negative ψ value (curve types 3 and 4 in Fig. 2). From equation (1), in order for ψ to be negative in the range $0° \leq \alpha \leq 90°$ then:

$$\cot(\theta_1) > 2\tan\left(\frac{\alpha}{2}\right) + \cot(\alpha + \theta_2) \qquad (1b)$$

APPENDIX B

Fault-bend fold theory extended: anti-listric faults

Fig. 4a illustrates an undeformed, horizontal bed resting against a segmented anti-listric fault surface. Fig. 4b illustrates the same bed after fault slip such that the whole of the bed has slipped past the fault bend.

Define angles

$$GA'H = \theta_2 - \alpha$$

$$outerA'HI = 180 + \alpha$$

therefore:

$$E'HI = A'HE' = \left(\frac{180 + \alpha}{2} \right) = 90 + \frac{\alpha}{2}$$

Line E'H must bisect angle A'HI as a consequence of the requirement of constant bed thickness (e.g., Suppe, 1985, page 63, Fig. 2-24), and defining angles in all the triangles within this angular bend fold gives the equality: $E'HI = A'HE'$.

and:

$$E'HF = \frac{\alpha}{2}$$

$$GE'H = 90 - \theta_2 + \frac{\alpha}{2}$$

$$HE'F = 90 - \frac{\alpha}{2}$$

Define lengths, assuming conservation of bed length:

$$BE = CD = t$$

$$AB = \frac{t}{\tan(\theta_1)}$$

$$E'F = t \cdot \tan\left(\frac{\alpha}{2}\right)$$

$$AC = l_0$$

$$ED = E'D' = l_0 - \frac{t}{\tan(\theta_1)}$$

$$IC' = t \cdot \tan(\psi)$$

$$A'H = l_0 - t \cdot \tan(\psi) - \left(l_0 - \frac{t}{\tan(\theta_1)} - t \cdot \tan\left(\frac{\alpha}{2}\right)\right) = t\left[\frac{1}{\tan(\theta_1)} + \tan\left(\frac{\alpha}{2}\right) - \tan(\psi)\right]$$

$$A'G = t\cdot\left(\frac{1}{\tan(\theta_1)} + \tan\left(\frac{\alpha}{2}\right) - \tan(\psi)\right)\cdot\cos(\theta_2 - \alpha)$$

$$HG = A'B = \sin(\theta_2 - \alpha) = t\cdot\sin(\theta_2 - \alpha)\cdot\left[\frac{1}{\tan(\theta_1)} + \tan\left(\frac{\alpha}{2}\right) - \tan(\psi)\right]$$

$$A'E' = \frac{\sin\left(90 + \frac{\alpha}{2}\right)\cdot t\cdot\left(\frac{1}{\tan(\theta_1)} + \tan\left(\frac{\alpha}{2}\right) - \tan(\psi)\right)}{\sin\left(90 - \theta_2 + \frac{\alpha}{2}\right)}$$

$$HI = l_0 - \frac{t}{\tan(\theta_1)} - t\cdot\tan\left(\frac{\alpha}{2}\right)$$

Undeformed area:

$$Area = t\left(l_0 - \frac{t}{\tan(\theta_1)}\right) + \frac{t^2}{2\cdot\tan(\theta_1)}$$

Deformed area:

$$AreaA'HG = \frac{\left[t\cdot\left(\frac{1}{\tan(\theta_1)} + \tan\left(\frac{\alpha}{2}\right) - \tan(\psi)\right)\right]^2\cdot\cos(\theta_2 - \alpha)\cdot\sin(\theta_s - \alpha)}{2}$$

$$AreaGHE' = \frac{\left[t\cdot\left(\frac{1}{\tan(\theta_1)} + \tan\left(\frac{\alpha}{2}\right) - \tan(\psi)\right)\right]\cdot\sin(\theta_2 - \alpha)\cdot(AD - AC)}{2}$$

$$AreaHE'F = \frac{t^2 \cdot \tan\left(\frac{\alpha}{2}\right)}{2}$$

$$AreaIC'D' = \frac{t^2 \cdot \tan(\psi)}{2}$$

$$AreaHID'F = t\left(l_0 - \frac{t}{\tan(\theta_1)} - t \cdot \tan\left(\frac{\alpha}{2}\right)\right)$$

Equate deformed and undeformed areas, substitute for l_0 and eliminate t, and simplifying gives equation (2):

$$\cot(\theta_1) = \tan(\psi) - \tan\left(\frac{\alpha}{2}\right) + \left[\frac{\sin(\theta_2 - \alpha) \cdot \cos\left(\frac{\alpha}{2}\right)}{\cos\left(\theta_2 - \frac{\alpha}{2}\right)}\right] \cdot \left[\cot(\theta_1) + \tan\left(\frac{\alpha}{2}\right) - \tan(\psi)\right]^2 \quad (2)$$

This equation can be solved numerically by fixing values for θ_1, θ_2, and varying α and ψ.

APPENDIX C

Steps for hangingwall construction based on fault shape alone.

(1) Figs 10a & b: Digitize the fault shape. Each point on the digitized line will be referred to as a node. Each straight-line section of the fault (between two nodes) is numbered from top to base, and has a dip of θ_n, where n is the fault section number (from 1 to N, in our example N = 6).

(2) Fig. 10c: Divide the undeformed hangingwall into segments by drawing horizontal lines from each of the fault nodes. Each segment and the horizon that marks its top will be referred to by the number of the fault section that bounds it in the undeformed state.

(3) Fig. 10d: Specify the displacement of the topmost horizon (horizon 1) along the fault.

(4) Fig. 10e: Determine which fault section the horizon 1 cutoff lies in, let this be F (in our example F = 2).

(5) i = 1. *(segment number)*

(6) j = F. *(fault section number)*

(7) k = 1. *(horizon number)*

(8) Initial cutoff angle = $\theta_1 = \theta_i$ (*dip of fault at the initial cutoff of horizon i*) (in our example, $\theta_1 = 60°$).

(9) Final resting angle = $\theta_2 = \theta_j$ (*final resting angle of horizon i*) (in our example, $\theta_2 = 50°$).

(10) Determine the minimum deformation α and ψ for this pair of θ values from Fig. 6 (in our example, $\alpha = 27°$, $\psi = 8°$).

(11) $\alpha_k = \alpha$

(12) Fig. 10f: Construct the top of segment i with a dip of α, from the deformed state cutoff point.

(13) Fig. 10f: Increment k by 1.

(14) Fig. 10f: Parallel-project downwards, the geometry of horizon i to the next fault node or the next horizon cutoff, whichever is next, call this point k.

(15) If fault node is next then:

(16) Fig. 10g: Increment j by 1. (in our example the point is a fault node)

Else:

(17) If cutoff is next then:

(18) Increment i by 1.

(19) Do (8) to (11) using the new values of i, j, and k (in our example, $\theta_1 = 60°$, $\theta_2 = 40°$).

(20) Fig. 10g: Construct the dip-domain boundary for the dip change $\alpha_{(k-1)}$ to α_k (in our example the forelimb dip changes from 27° to 33°).

(21) Fig. 10g: Attach this dip-domain boundary to the fault at point k.

(22) Fig. 10h: Modify the horizon dips across this dip-domain boundary to match the dips $\alpha_{(k-1)}$ and α_k.

(23) Repeat (13) to (23) until the bottom of the hangingwall is reached.

(24) Fig. 10i: Construct form lines parallel to the layer geometry extending from each of the points "k".

(25) Fig. 10i: At a point in the hangingwall where all form lines are horizontal (or parallel to the main detachment fault), choose a point in the uppermost line and construct the shear profile using the ψ values obtained from the above algorithm.

APPENDIX D

Steps to construct shear strain profile construction based on fault shape and hangingwall geometry.

(1) Digitize the fault shape. Each point on the digitized line will be referred to as a node. Each straight-line section of the fault (between two nodes) is numbered from top to base, and has a dip of θ_n, where n is the fault section number (from 1 to N).

(2) Divide the undeformed hangingwall into segments by drawing horizontal lines from each of the fault nodes. Each segment and the horizon that marks its top will be referred to by the number of the fault section that bounds it in the undeformed state.

(3) Using the deformed shape of the uppermost horizon, parallel-project its geometry downward to the base of the hangingwall sequence, constructing layer-parallel form lines wherever there is a change in fault dip or a horizon intersects the fault.

(4) Determine which fault section the horizon 1 cutoff lies in, let this be F.

(5) $i = 1$

(6) $j = F$

(7) $k = 1$

(8) Measure the dip of the hangingwall at the cutoff point, this is α

(9) $\theta_1 = \theta_i$

(10) $\theta_2 = \theta_j$

(11) Determine the ψ value for the α and θ values (Fig. 5).

(12) $\alpha_k = \alpha$

(13) Increment k by 1.

(14) Move down the fault to the next form line cutoff, call this point k.

(15) If fault node is next then:

(16) Increment j by 1.

(17) If cutoff is next then:

(18) Increment i by 1.

(19) Do (8) to (12).

(20) Repeat (13) to (19) until the bottom of the hangingwall is reached.

(21) At a point in the hangingwall where all form lines are horizontal (or parallel to the main detachment fault), choose a point in the uppermost line and construct the shear profile using the ψ values obtained from the above algorithm.

Figure Captions

Fig. 1. Angular elements of listric normal fault and hangingwall used to derive equation (1).

Fig. 2. Examples of the four curve types from solutions to equation (1).

(a) Type 1: Single minimum, only positive shear in the range of $-90° < \psi < 90°$.

(b) Type 2: Double minimum, one at $\psi = 0$, the other at some higher ψ value, but lower α value.

(c) Type 3: Single minimum, both positive and negative shear in the range of $-90° < \psi < 90°$.

(d) Type 4: Double minimum, both minima are at $\psi = 0$.

Fig. 3. Graphs of α (forelimb dip) against ψ (layer-parallel shear) for eight sets of solutions to equation (1) for an initial cutoff angle of 80°. Curves for final resting angles of 70° through 40° (representing increased displacement for a listric normal fault) are shown. The locus of minimum shear is also plotted, illustrating the continuity of the minimum shear solution with the Type 4 curve minimum at $\alpha = 13°$, $\psi = 10°$.

Fig. 4. Angular elements of antilistric normal fault and hangingwall used to derive equation (2).

Fig. 5. Reference graphs of forelimb dip (α) versus layer-parallel shear (ψ) for initial cutoff angles (θ_1) from 10° to 80° in 10° increments, and for final resting angles (θ_2) from 0° to 90° in 10° increments. Equation (1) is solved to draw the listric solutions, and equation (2) is solved to draw the anti-listric solutions.

Fig. 6. Minimum deformation solutions.

(a) Graph showing the θ_1, θ_2 domains for which minimum deformation solutions can be obtained.

(b) Table of minimum deformation α values for the complete range of θ_1, θ_2 values.

Fig. 7. An example of a forward-modeled listric normal fault (see text). (a) Undeformed hangingwall. (b) Deformed hangingwall constructed using the principle of minimum deformation.

Fig. 8. Fault trajectory prediction from hangingwall geometry using minimum deformation approach.

(a) Deformed state: the fault trajectory from footwall cutoff to hangingwall cutoff is known, as is the shape of the top of horizon 1 in the hangingwall. Because segment 1 can be restored as shown in (b), the cutoff angle (θ_1) for segment 1 is 70°, and the forelimb dip is 20°.

(b) Restored state of (a).

(c) Deformed state: knowing that the cutoff angle of segment 1 is 70°and that it now has dip of 20°, using Fig. 6 we see that this corresponds to a final resting angle (θ_2) of 60°.

Therefore the fault trajectory in the deformed state can be continued downward at a dip of 60°.

(d) Restored state of (c).

(e) Deformed state: knowing that the cutoff angle of segment 2 is 60°and that it now has dip of 20°, using Fig. 6 we see that this corresponds to a final resting angle (θ_2) of between 57° and 58°. Because the dip value for a final resting angle of 57° (22°) is much closer than that for 58° (11°) the fault trajectory in the deformed state can be continued downward at a dip of 57°.

(f) Restored state of (e).

Fig. 9. An example of a sequentially forward-modeled listric normal fault (see text).

Fig. 10. (a) through (i) illustrate the steps required forward-model hangingwall geometry on a known or assumed fault shape. See appendix C for full description.

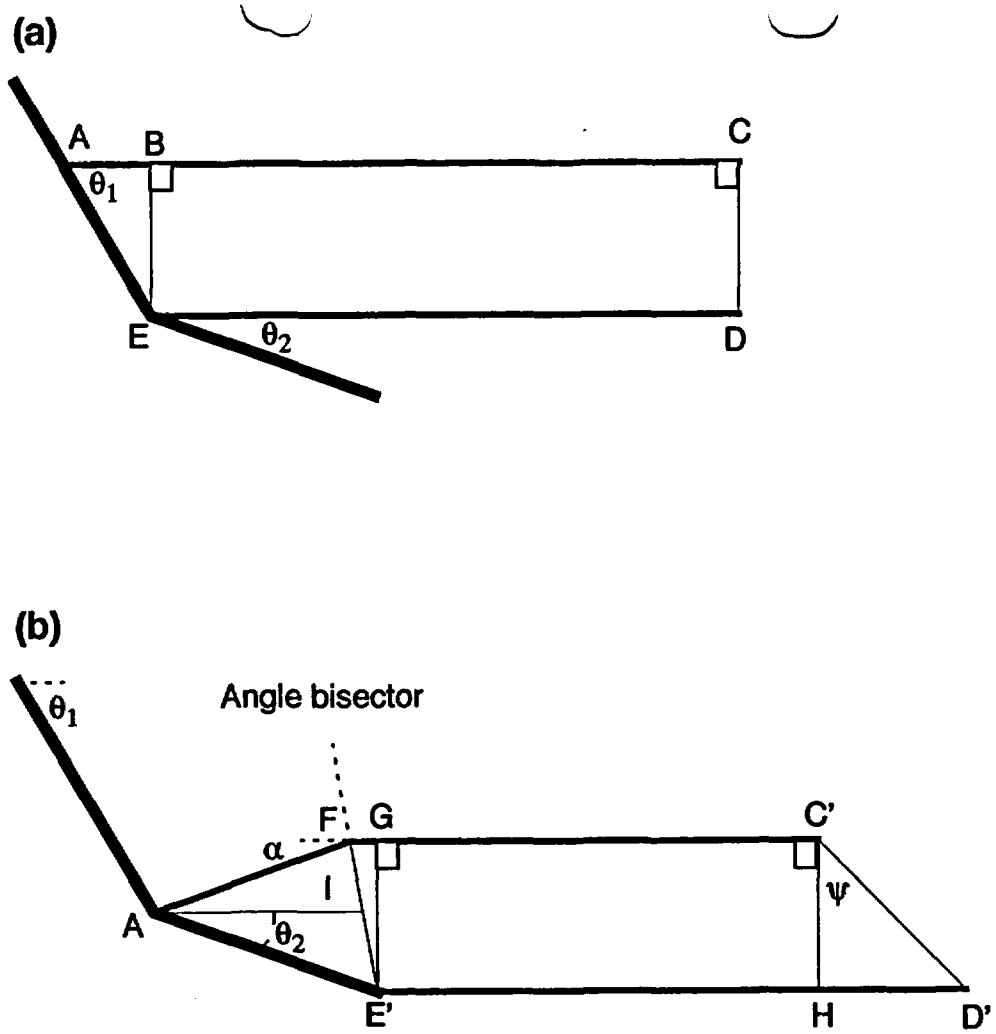

Morris and Ferrill Fig. 1

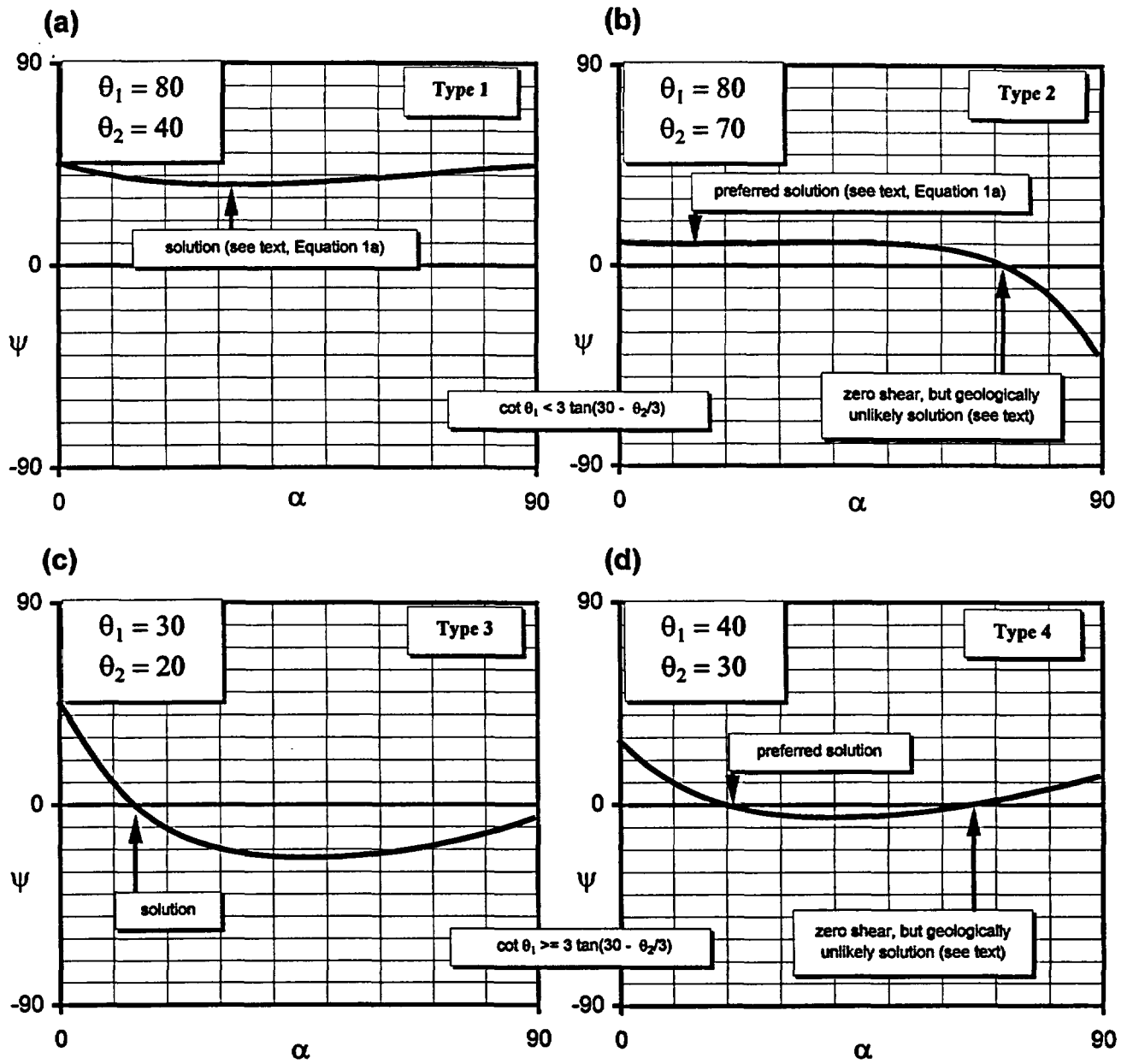

Morris and Ferrill Fig.2

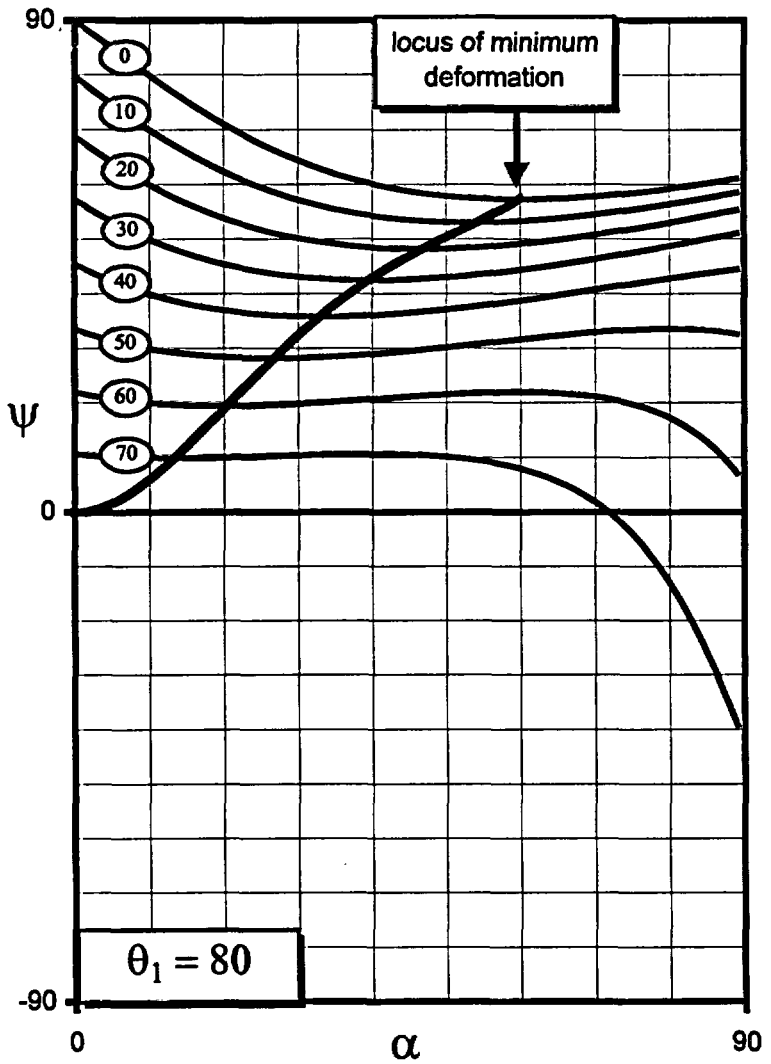

Morris and Ferrill Fig. 3

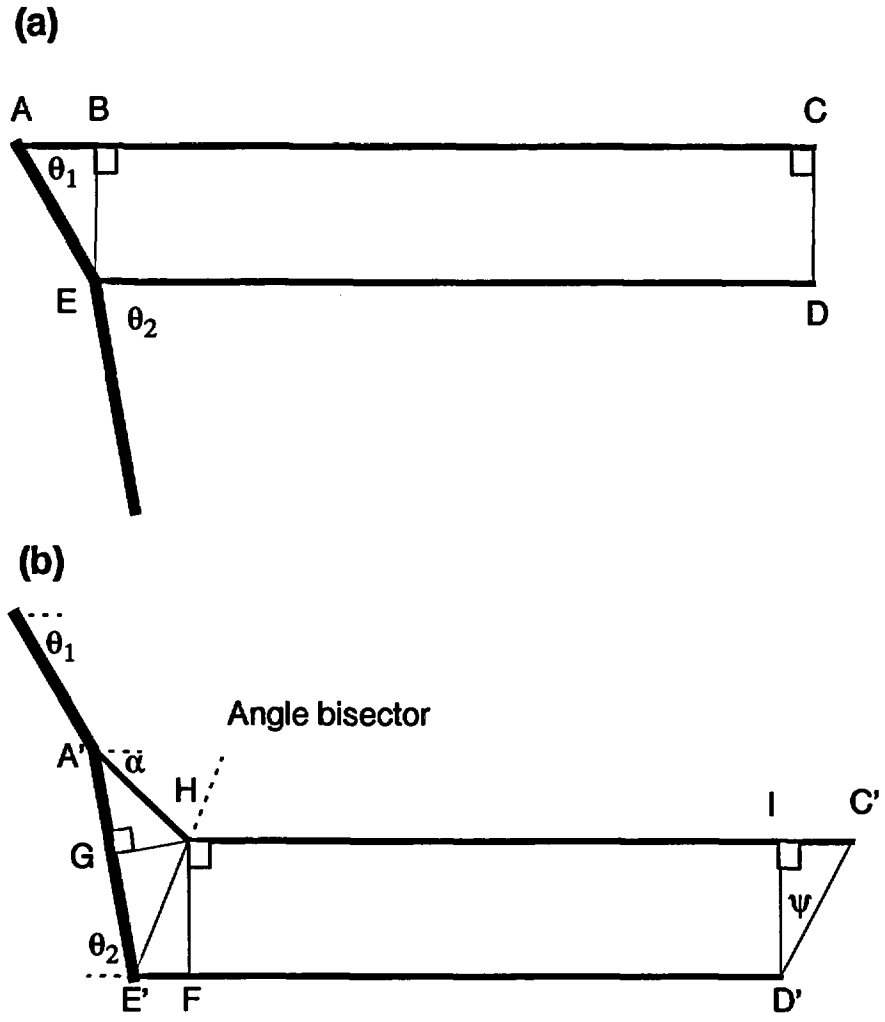

Morris and Ferrill Fig. 4

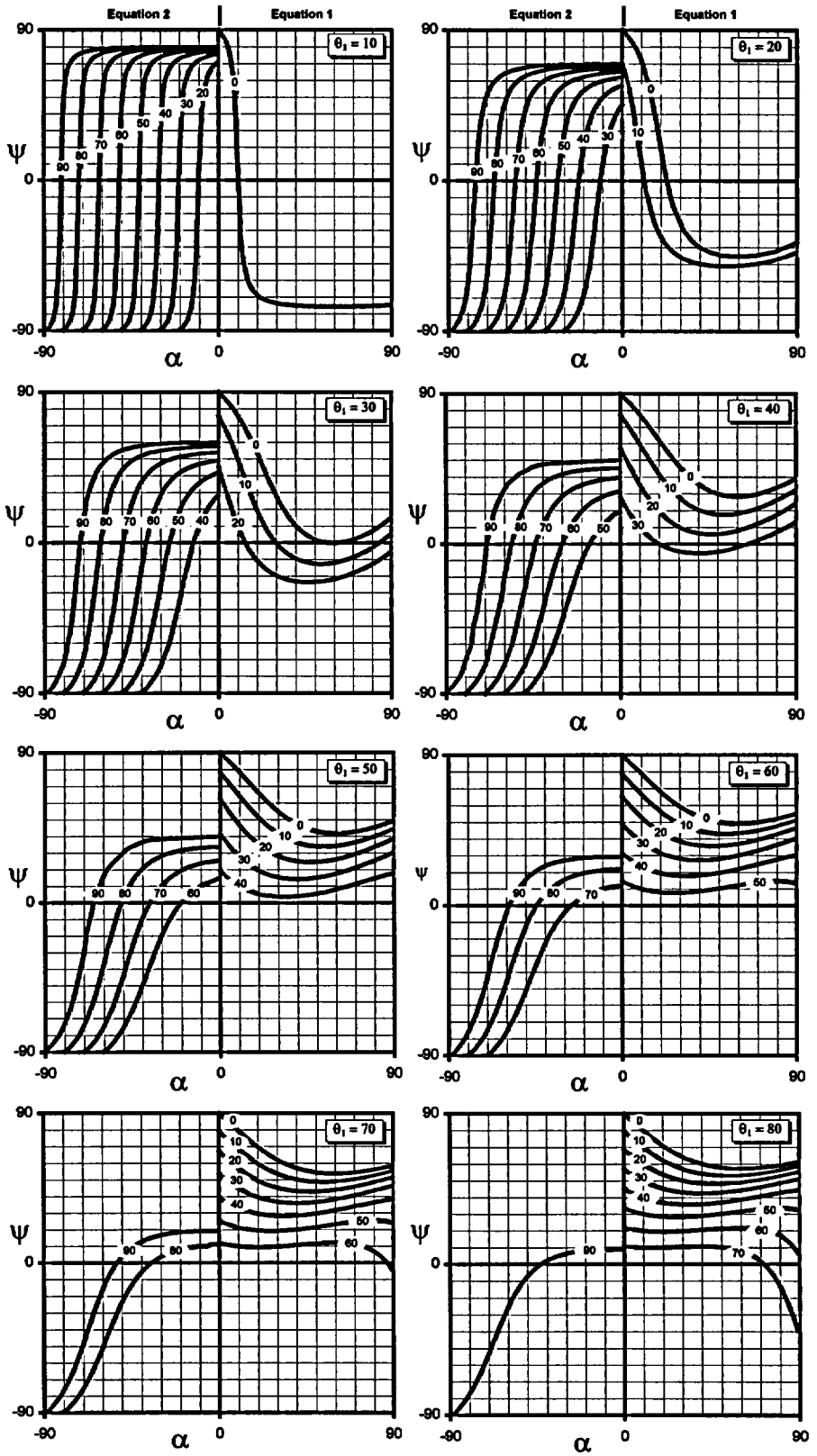

Morris and Ferrill Fig. 5

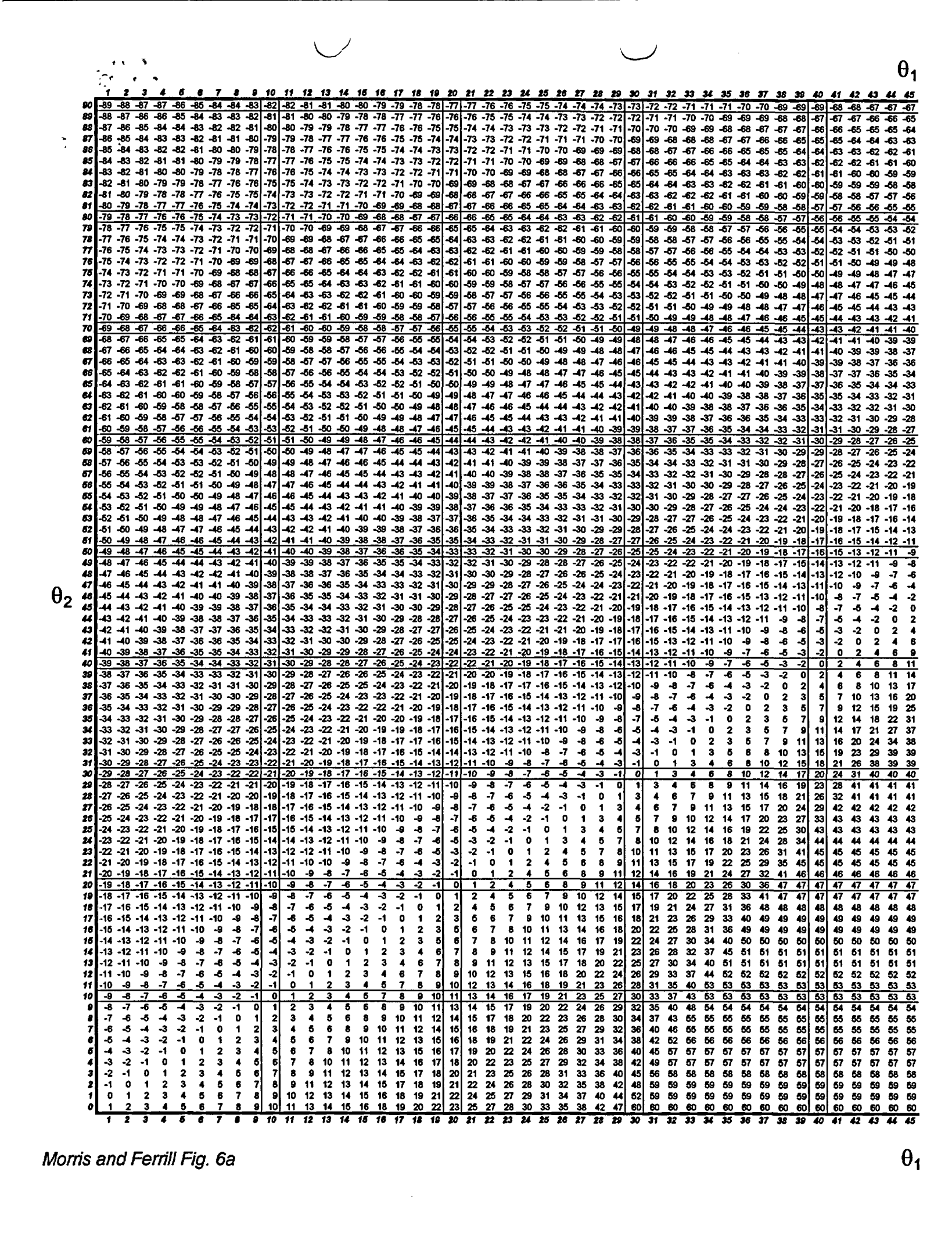

Morris and Ferrill Fig. 6a

46	47	48	49	50	51	52	53	54	55	56	57	58	59	60	61	62	63	64	65	66	67	68	69	70	71	72	73	74	75	76	77	78	79	80	81	82	83	84	85	86	87	88	89	90	θ_2
-66	-66	-65	-65	-65	-64	-64	-63	-63	-62	-62	-62	-61	-61	-60	-60	-59	-58	-58	-57	-57	-56	-56	-55	-54	-54	-53	-52	-51	-50	-50	-49	-48	-47	-45	-44	-43	-41	-39	-37	-35	-32	-29	-23	0	90
-65	-65	-64	-64	-63	-63	-62	-62	-61	-61	-61	-60	-60	-59	-59	-58	-57	-57	-56	-56	-55	-55	-54	-53	-53	-52	-51	-50	-49	-48	-47	-46	-45	-44	-43	-42	-40	-38	-36	-34	-31	-27	-22	0	1	89
-64	-63	-63	-62	-62	-61	-61	-61	-60	-60	-59	-59	-58	-58	-57	-56	-56	-55	-55	-54	-53	-53	-52	-51	-51	-50	-49	-48	-47	-46	-45	-44	-43	-42	-40	-39	-37	-35	-33	-30	-26	-20	0	1	1	88
-62	-62	-61	-61	-61	-60	-60	-59	-59	-58	-58	-57	-57	-56	-55	-55	-54	-54	-53	-52	-52	-51	-50	-50	-49	-48	-47	-46	-45	-44	-43	-42	-41	-39	-38	-36	-34	-31	-29	-25	-19	0	2	2	2	87
-61	-61	-60	-60	-59	-59	-58	-58	-57	-57	-56	-56	-55	-55	-54	-53	-53	-52	-51	-51	-50	-49	-49	-48	-47	-46	-45	-44	-43	-42	-41	-40	-38	-37	-35	-33	-30	-27	-24	-18	0	3	3	3	3	86
-60	-59	-59	-58	-58	-57	-57	-56	-56	-55	-55	-54	-54	-53	-52	-52	-51	-50	-50	-49	-48	-48	-47	-46	-45	-44	-43	-42	-41	-40	-38	-37	-35	-34	-32	-29	-26	-23	-17	0	3	3	3	3	3	85
-58	-58	-57	-57	-56	-56	-55	-55	-54	-54	-53	-53	-52	-51	-51	-50	-50	-49	-48	-47	-47	-46	-45	-44	-43	-42	-41	-40	-39	-37	-36	-34	-33	-31	-28	-25	-21	-16	0	4	4	4	4	4	4	84
-57	-57	-56	-56	-55	-55	-54	-53	-53	-52	-52	-51	-51	-50	-49	-49	-48	-47	-46	-46	-45	-44	-43	-42	-41	-40	-39	-38	-36	-35	-33	-31	-29	-27	-24	-20	-15	0	5	5	5	5	5	5	5	83
-56	-55	-55	-54	-54	-53	-53	-52	-51	-51	-50	-50	-49	-48	-48	-47	-46	-45	-45	-44	-43	-42	-41	-40	-39	-38	-37	-35	-34	-32	-30	-28	-26	-23	-19	-14	0	5	5	5	5	5	5	5	5	82
-54	-54	-53	-53	-52	-52	-51	-51	-50	-49	-49	-48	-47	-47	-46	-45	-44	-44	-43	-42	-41	-40	-39	-38	-37	-36	-34	-33	-31	-29	-27	-25	-22	-18	-13	0	6	6	6	6	6	6	6	6	6	81
-53	-53	-52	-51	-51	-50	-50	-49	-48	-48	-47	-46	-46	-45	-44	-44	-43	-42	-41	-40	-39	-38	-37	-36	-35	-33	-32	-30	-28	-26	-24	-21	-18	-12	0	7	7	7	7	7	7	7	7	7	7	80
-52	-51	-51	-50	-49	-49	-48	-48	-47	-46	-46	-45	-44	-43	-43	-42	-41	-40	-39	-38	-37	-36	-35	-34	-32	-31	-29	-28	-25	-23	-20	-17	-11	0	7	7	7	7	7	7	7	7	7	7	7	79
-50	-50	-49	-49	-48	-47	-47	-46	-45	-45	-44	-43	-43	-42	-41	-40	-39	-38	-37	-36	-35	-34	-33	-31	-30	-28	-27	-25	-22	-19	-16	-11	0	8	8	8	8	8	8	8	8	8	8	8	8	78
-49	-48	-48	-47	-47	-46	-45	-45	-44	-43	-42	-42	-41	-40	-39	-38	-37	-36	-35	-34	-33	-32	-31	-29	-27	-26	-24	-21	-18	-15	-10	0	9	9	9	9	9	9	9	9	9	9	9	9	9	77
-48	-47	-46	-46	-45	-44	-44	-43	-42	-42	-41	-40	-39	-38	-38	-37	-36	-35	-33	-32	-31	-30	-28	-27	-25	-23	-20	-18	-14	-9	0	9	9	9	9	9	9	9	9	9	9	9	9	9	9	76
-46	-46	-45	-44	-44	-43	-42	-42	-41	-40	-39	-38	-38	-37	-36	-35	-34	-33	-31	-30	-29	-27	-26	-24	-22	-20	-17	-13	-9	0	10	10	10	10	10	10	10	10	10	10	10	10	10	10	10	75
-45	-44	-44	-43	-42	-41	-41	-40	-39	-38	-38	-37	-36	-35	-34	-33	-32	-31	-29	-28	-27	-25	-23	-21	-19	-16	-13	-8	0	11	11	11	11	11	11	11	11	11	11	11	11	11	11	11	11	74
-43	-43	-42	-41	-41	-40	-39	-38	-38	-37	-36	-35	-34	-33	-32	-31	-30	-29	-27	-26	-24	-22	-20	-18	-15	-12	-8	0	11	11	11	11	11	11	11	11	11	11	11	11	11	11	11	11	11	73
-42	-41	-41	-40	-39	-38	-38	-37	-36	-35	-34	-33	-32	-31	-30	-29	-28	-26	-25	-23	-22	-20	-17	-15	-11	-7	0	12	12	12	12	12	12	12	12	12	12	12	12	12	12	12	12	12	12	72
-41	-40	-39	-39	-38	-37	-36	-35	-34	-34	-33	-32	-31	-29	-28	-27	-26	-24	-23	-21	-19	-17	-14	-11	-7	0	13	13	13	13	13	13	13	13	13	13	13	13	13	13	13	13	13	13	13	71
-39	-39	-38	-37	-36	-35	-35	-34	-33	-32	-31	-30	-29	-27	-26	-25	-23	-22	-20	-18	-16	-13	-10	-6	0	13	13	13	13	13	13	13	13	13	13	13	13	13	13	13	13	13	13	13	13	70
-38	-37	-36	-36	-35	-34	-33	-32	-31	-30	-29	-28	-27	-26	-24	-23	-21	-19	-18	-15	-13	-10	-6	0	14	14	14	14	14	14	14	14	14	14	14	14	14	14	14	14	14	14	14	14	14	69
-36	-36	-35	-34	-33	-32	-31	-30	-29	-28	-27	-26	-25	-24	-22	-21	-19	-17	-15	-12	-9	-6	0	15	15	15	15	15	15	15	15	15	15	15	15	15	15	15	15	15	15	15	15	15	15	68
-35	-34	-33	-32	-32	-31	-30	-29	-28	-27	-25	-24	-23	-21	-20	-18	-16	-14	-12	-9	-5	0	14	15	15	15	15	15	15	15	15	15	15	15	15	15	15	15	15	15	15	15	15	15	15	67
-34	-33	-32	-31	-30	-29	-28	-27	-26	-25	-24	-22	-21	-19	-18	-16	-14	-11	-8	-5	0	10	16	16	16	16	16	16	16	16	16	16	16	16	16	16	16	16	16	16	16	16	16	16	16	66
-32	-31	-30	-29	-28	-27	-26	-25	-24	-23	-22	-20	-19	-17	-15	-13	-11	-8	-5	0	8	17	17	17	17	17	17	17	17	17	17	17	17	17	17	17	17	17	17	17	17	17	17	17	17	65
-31	-30	-29	-28	-27	-26	-25	-23	-22	-21	-20	-18	-16	-15	-13	-10	-8	-4	0	7	17	17	17	17	17	17	17	17	17	17	17	17	17	17	17	17	17	17	17	17	17	17	17	17	17	64
-29	-28	-27	-26	-25	-24	-23	-22	-20	-19	-18	-16	-14	-12	-10	-7	-4	0	6	18	18	18	18	18	18	18	18	18	18	18	18	18	18	18	18	18	18	18	18	18	18	18	18	18	18	63
-28	-27	-26	-25	-23	-22	-21	-20	-18	-17	-15	-14	-12	-10	-7	-4	0	6	19	19	19	19	19	19	19	19	19	19	19	19	19	19	19	19	19	19	19	19	19	19	19	19	19	19	19	62
-26	-25	-24	-23	-22	-21	-19	-18	-16	-15	-13	-11	-9	-7	-4	0	5	19	19	19	19	19	19	19	19	19	19	19	19	19	19	19	19	19	19	19	19	19	19	19	19	19	19	19	19	61
-24	-23	-22	-21	-20	-19	-17	-16	-14	-13	-11	-9	-6	-4	0	5	15	20	20	20	20	20	20	20	20	20	20	20	20	20	20	20	20	20	20	20	20	20	20	20	20	20	20	20	20	60
-23	-22	-21	-20	-18	-17	-16	-14	-12	-10	-8	-6	-3	0	5	12	21	21	21	21	21	21	21	21	21	21	21	21	21	21	21	21	21	21	21	21	21	21	21	21	21	21	21	21	21	59
-21	-20	-19	-18	-16	-15	-14	-12	-10	-8	-6	-3	0	4	11	21	21	21	21	21	21	21	21	21	21	21	21	21	21	21	21	21	21	21	21	21	21	21	21	21	21	21	21	21	21	58
-20	-19	-17	-16	-15	-13	-12	-10	-8	-6	-3	0	4	10	22	22	22	22	22	22	22	22	22	22	22	22	22	22	22	22	22	22	22	22	22	22	22	22	22	22	22	22	22	22	22	57
-18	-17	-16	-14	-13	-11	-9	-8	-5	-3	0	4	9	23	23	23	23	23	23	23	23	23	23	23	23	23	23	23	23	23	23	23	23	23	23	23	23	23	23	23	23	23	23	23	23	56
-16	-15	-14	-12	-11	-9	-7	-5	-3	0	3	8	16	23	23	23	23	23	23	23	23	23	23	23	23	23	23	23	23	23	23	23	23	23	23	23	23	23	23	23	23	23	23	23	23	55
-15	-13	-12	-11	-9	-7	-5	-3	0	3	7	14	24	24	24	24	24	24	24	24	24	24	24	24	24	24	24	24	24	24	24	24	24	24	24	24	24	24	24	24	24	24	24	24	24	54
-13	-12	-10	-9	-7	-5	-3	0	3	7	13	25	25	25	25	25	25	25	25	25	25	25	25	25	25	25	25	25	25	25	25	25	25	25	25	25	25	25	25	25	25	25	25	25	25	53
-11	-10	-8	-7	-5	-2	0	3	7	11	24	25	25	25	25	25	25	25	25	25	25	25	25	25	25	25	25	25	25	25	25	25	25	25	25	25	25	25	25	25	25	25	25	25	25	52
-10	-8	-6	-4	-2	0	3	6	11	18	26	26	26	26	26	26	26	26	26	26	26	26	26	26	26	26	26	26	26	26	26	26	26	26	26	26	26	26	26	26	26	26	26	26	26	51
-8	-6	-4	-2	0	3	6	10	16	27	27	27	27	27	27	27	27	27	27	27	27	27	27	27	27	27	27	27	27	27	27	27	27	27	27	27	27	27	27	27	27	27	27	27	27	50
-6	-4	-2	0	3	6	9	14	27	27	27	27	27	27	27	27	27	27	27	27	27	27	27	27	27	27	27	27	27	27	27	27	27	27	27	27	27	27	27	27	27	27	27	27	27	49
-4	-2	0	2	5	9	13	22	28	28	28	28	28	28	28	28	28	28	28	28	28	28	28	28	28	28	28	28	28	28	28	28	28	28	28	28	28	28	28	28	28	28	28	28	28	48
-2	0	2	5	8	12	19	29	29	29	29	29	29	29	29	29	29	29	29	29	29	29	29	29	29	29	29	29	29	29	29	29	29	29	29	29	29	29	29	29	29	29	29	29	29	47
0	2	5	8	11	17	29	29	29	29	29	29	29	29	29	29	29	29	29	29	29	29	29	29	29	29	29	29	29	29	29	29	29	29	29	29	29	29	29	29	29	29	29	29	29	46
2	5	7	11	15	24	30	30	30	30	30	30	30	30	30	30	30	30	30	30	30	30	30	30	30	30	30	30	30	30	30	30	30	30	30	30	30	30	30	30	30	30	30	30	30	45
4	7	10	14	20	31	31	31	31	31	31	31	31	31	31	31	31	31	31	31	31	31	31	31	31	31	31	31	31	31	31	31	31	31	31	31	31	31	31	31	31	31	31	31	31	44
7	10	13	18	31	31	31	31	31	31	31	31	31	31	31	31	31	31	31	31	31	31	31	31	31	31	31	31	31	31	31	31	31	31	31	31	31	31	31	31	31	31	31	31	31	43
9	13	17	24	32	32	32	32	32	32	32	32	32	32	32	32	32	32	32	32	32	32	32	32	32	32	32	32	32	32	32	32	32	32	32	32	32	32	32	32	32	32	32	32	32	42
12	16	22	33	33	33	33	33	33	33	33	33	33	33	33	33	33	33	33	33	33	33	33	33	33	33	33	33	33	33	33	33	33	33	33	33	33	33	33	33	33	33	33	33	33	41
15	20	30	33	33	33	33	33	33	33	33	33	33	33	33	33	33	33	33	33	33	33	33	33	33	33	33	33	33	33	33	33	33	33	33	33	33	33	33	33	33	33	33	33	33	40
18	25	34	34	34	34	34	34	34	34	34	34	34	34	34	34	34	34	34	34	34	34	34	34	34	34	34	34	34	34	34	34	34	34	34	34	34	34	34	34	34	34	34	34	34	39
22	35	35	35	35	35	35	35	35	35	35	35	35	35	35	35	35	35	35	35	35	35	35	35	35	35	35	35	35	35	35	35	35	35	35	35	35	35	35	35	35	35	35	35	35	38
28	35	35	35	35	35	35	35	35	35	35	35	35	35	35	35	35	35	35	35	35	35	35	35	35	35	35	35	35	35	35	35	35	35	35	35	35	35	35	35	35	35	35	35	35	37
36	36	36	36	36	36	36	36	36	36	36	36	36	36	36	36	36	36	36	36	36	36	36	36	36	36	36	36	36	36	36	36	36	36	36	36	36	36	36	36	36	36	36	36	36	36
37	37	37	37	37	37	37	37	37	37	37	37	37	37	37	37	37	37	37	37	37	37	37	37	37	37	37	37	37	37	37	37	37	37	37	37	37	37	37	37	37	37	37	37	37	35
37	37	37	37	37	37	37	37	37	37	37	37	37	37	37	37	37	37	37	37	37	37	37	37	37	37	37	37	37	37	37	37	37	37	37	37	37	37	37	37	37	37	37	37	37	34
38	38	38	38	38	38	38	38	38	38	38	38	38	38	38	38	38	38	38	38	38	38	38	38	38	38	38	38	38	38	38	38	38	38	38	38	38	38	38	38	38	38	38	38	38	33
39	39	39	39	39	39	39	39	39	39	39	39	39	39	39	39	39	39	39	39	39	39	39	39	39	39	39	39	39	39	39	39	39	39	39	39	39	39	39	39	39	39	39	39	39	32
39	39	39	39	39	39	39	39	39	39	39	39	39	39	39	39	39	39	39	39	39	39	39	39	39	39	39	39	39	39	39	39	39	39	39	39	39	39	39	39	39	39	39	39	39	31
40	40	40	40	40	40	40	40	40	40	40	40	40	40	40	40	40	40	40	40	40	40	40	40	40	40	40	40	40	40	40	40	40	40	40	40	40	40	40	40	40	40	40	40	40	30
41	41	41	41	41	41	41	41	41	41	41	41	41	41	41	41	41	41	41	41	41	41	41	41	41	41	41	41	41	41	41	41	41	41	41	41	41	41	41	41	41	41	41	41	41	29
41	41	41	41	41	41	41	41	41	41	41	41	41	41	41	41	41	41	41	41	41	41	41	41	41	41	41	41	41	41	41	41	41	41	41	41	41	41	41	41	41	41	41	41	41	28
42	42	42	42	42	42	42	42	42	42	42	42	42	42	42	42	42	42	42	42	42	42	42	42	42	42	42	42	42	42	42	42	42	42	42	42	42	42	42	42	42	42	42	42	42	27
43	43	43	43	43	43	43	43	43	43	43	43	43	43	43	43	43	43	43	43	43	43	43	43	43	43	43	43	43	43	43	43	43	43	43	43	43	43	43	43	43	43	43	43	43	26
43	43	43	43	43	43	43	43	43	43	43	43	43	43	43	43	43	43	43	43	43	43	43	43	43	43	43	43	43	43	43	43	43	43	43	43	43	43	43	43	43	43	43	43	43	25
44	44	44	44	44	44	44	44	44	44	44	44	44	44	44	44	44	44	44	44	44	44	44	44	44	44	44	44	44	44	44	44	44	44	44	44	44	44	44	44	44	44	44	44	44	24
45	45	45	45	45	45	45	45	45	45	45	45	45	45	45	45	45	45	45	45	45	45	45	45	45	45	45	45	45	45	45	45	45	45	45	45	45	45	45	45	45	45	45	45	45	23
45	45	45	45	45	45	45	45	45	45	45	45	45	45	45	45	45	45	45	45	45	45	45	45	45	45	45	45	45	45	45	45	45	45	45	45	45	45	45	45	45	45	45	45	45	22
46	46	46	46	46	46	46	46	46	46	46	46	46	46	46	46	46	46	46	46	46	46	46	46	46	46	46	46	46	46	46	46	46	46	46	46	46	46	46	46	46	46	46	46	46	21
47	47	47	47	47	47	47	47	47	47	47	47	47	47	47	47	47	47	47	47	47	47	47	47	47	47	47	47	47	47	47	47	47	47	47	47	47	47	47	47	47	47	47	47	47	20
47	47	47	47	47	47	47	47	47	47	47	47	47	47	47	47	47	47	47	47	47	47	47	47	47	47	47	47	47	47	47	47	47	47	47	47	47	47	47	47	47	47	47	47	47	19
48	48	48	48	48	48	48	48	48	48	48	48	48	48	48	48	48	48	48	48	48	48	48	48	48	48	48	48	48	48	48	48	48	48	48	48	48	48	48	48	48	48	48	48	48	18
49	49	49	49	49	49	49	49	49	49	49	49	49	49	49	49	49	49	49	49	49	49	49	49	49	49	49	49	49	49	49	49	49	49	49	49	49	49	49	49	49	49	49	49	49	17
49	49	49	49	49	49	49	49	49	49	49	49	49	49	49	49	49	49	49	49	49	49	49	49	49	49	49	49	49	49	49	49	49	49	49	49	49	49	49	49	49	49	49	49	49	16
50	50	50	50	50	50	50	50	50	50	50	50	50	50	50	50	50	50	50	50	50	50	50	50	50	50	50	50	50	50	50	50	50	50	50	50	50	50	50	50	50	50	50	50	50	15
51	51	51	51	51	51	51	51	51	51	51	51	51	51	51	51	51	51	51	51	51	51	51	51	51	51	51	51	51	51	51	51	51	51	51	51	51	51	51	51	51	51	51	51	51	14
51	51	51	51	51	51	51	51	51	51	51	51	51	51	51	51	51	51	51	51	51	51	51	51	51	51	51	51	51	51	51	51	51	51	51	51	51	51	51	51	51	51	51	51	51	13
52	52	52	52	52	52	52	52	52	52	52	52	52	52	52	52	52	52	52	52	52	52	52	52	52	52	52	52	52	52	52	52	52	52	52	52	52	52	52	52	52	52	52	52	52	12
53	53	53	53	53	53	53	53	53	53	53	53	53	53	53	53	53	53	53	53	53	53	53	53	53	53	53	53	53	53	53	53	53	53	53	53	53	53	53	53	53	53	53	53	53	11
53	53	53	53	53	53	53	53	53	53	53	53	53	53	53	53	53	53	53	53	53	53	53	53	53	53	53	53	53	53	53	53	53	53	53	53	53	53	53	53	53	53	53	53	53	10
54	54	54	54	54	54	54	54	54	54	54	54	54	54	54	54	54	54	54	54	54	54	54	54	54	54	54	54	54	54	54	54	54	54	54	54	54	54	54	54	54	54	54	54	54	9
55	55	55	55	55	55	55	55	55	55	55	55	55	55	55	55	55	55	55	55	55	55	55	55	55	55	55	55	55	55	55	55	55	55	55	55	55	55	55	55	55	55	55	55	55	8
55	55	55	55	55	55	55	55	55	55	55	55	55	55	55	55	55	55	55	55	55	55	55	55	55	55	55	55	55	55	55	55	55	55	55	55	55	55	55	55	55	55	55	55	55	7
56	56	56	56	56	56	56	56	56	56	56	56	56	56	56	56	56	56	56	56	56	56	56	56	56	56	56	56	56	56	56	56	56	56	56	56	56	56	56	56	56	56	56	56	56	6
57	57	57	57	57	57	57	57	57	57	57	57	57	57	57	57	57	57	57	57	57	57	57	57	57	57	57	57	57	57	57	57	57	57	57	57	57	57	57	57	57	57	57	57	57	5
57	57	57	57	57	57	57	57	57	57	57	57	57	57	57	57	57	57	57	57	57	57	57	57	57	57	57	57	57	57	57	57	57	57	57	57	57	57	57	57	57	57	57	57	57	4
58	58	58	58	58	58	58	58	58	58	58	58	58	58	58	58	58	58	58	58	58	58	58	58	58	58	58	58	58	58	58	58	58	58	58	58	58	58	58	58	58	58	58	58	58	3
59	59	59	59	59	59	59	59	59	59	59	59	59	59	59	59	59	59	59	59	59	59	59	59	59	59	59	59	59	59	59	59	59	59	59	59	59	59	59	59	59	59	59	59	59	2
59	59	59	59	59	59	59	59	59	59	59	59	59	59	59	59	59	59	59	59	59	59	59	59	59	59	59	59	59	59	59	59	59	59	59	59	59	59	59	59	59	59	59	59	59	1
60	60	60	60	60	60	60	60	60	60	60	60	60	60	60	60	60	60	60	60	60	60	60	60	60	60	60	60	60	60	60	60	60	60	60	60	60	60	60	60	60	60	60	60	60	0
46	47	48	49	50	51	52	53	54	55	56	57	58	59	60	61	62	63	64	65	66	67	68	69	70	71	72	73	74	75	76	77	78	79	80	81	82	83	84	85	86	87	88	89	90	

1

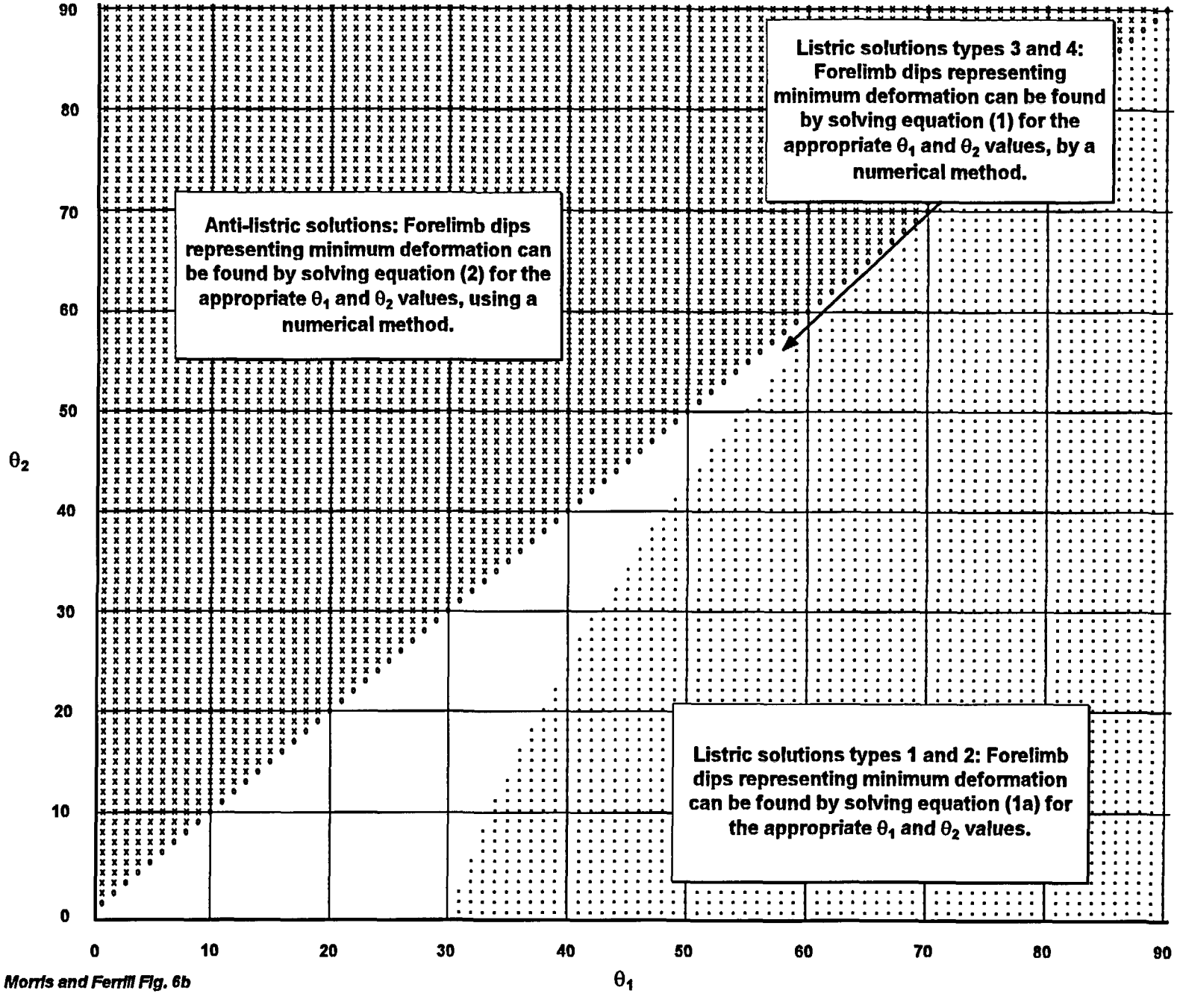

Morris and Ferrill Fig. 6b

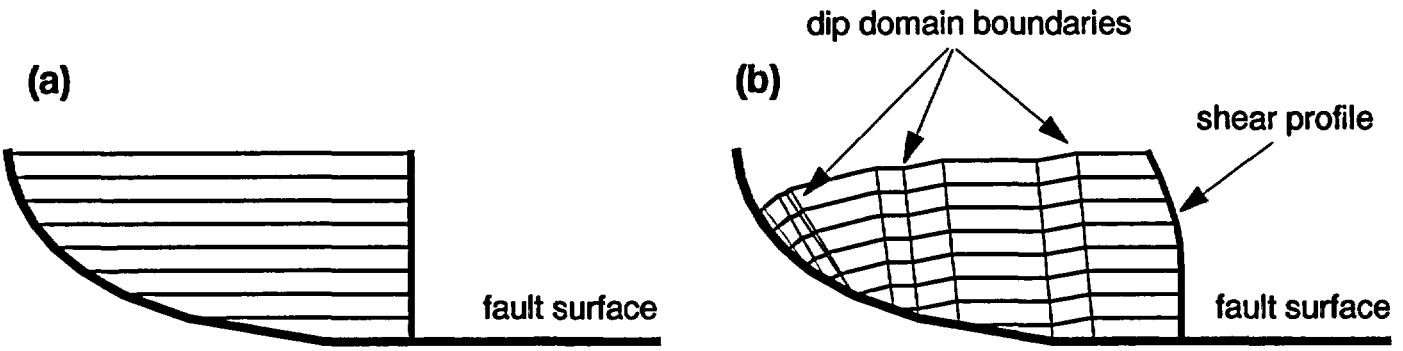

Morris and Ferrill Fig. 7

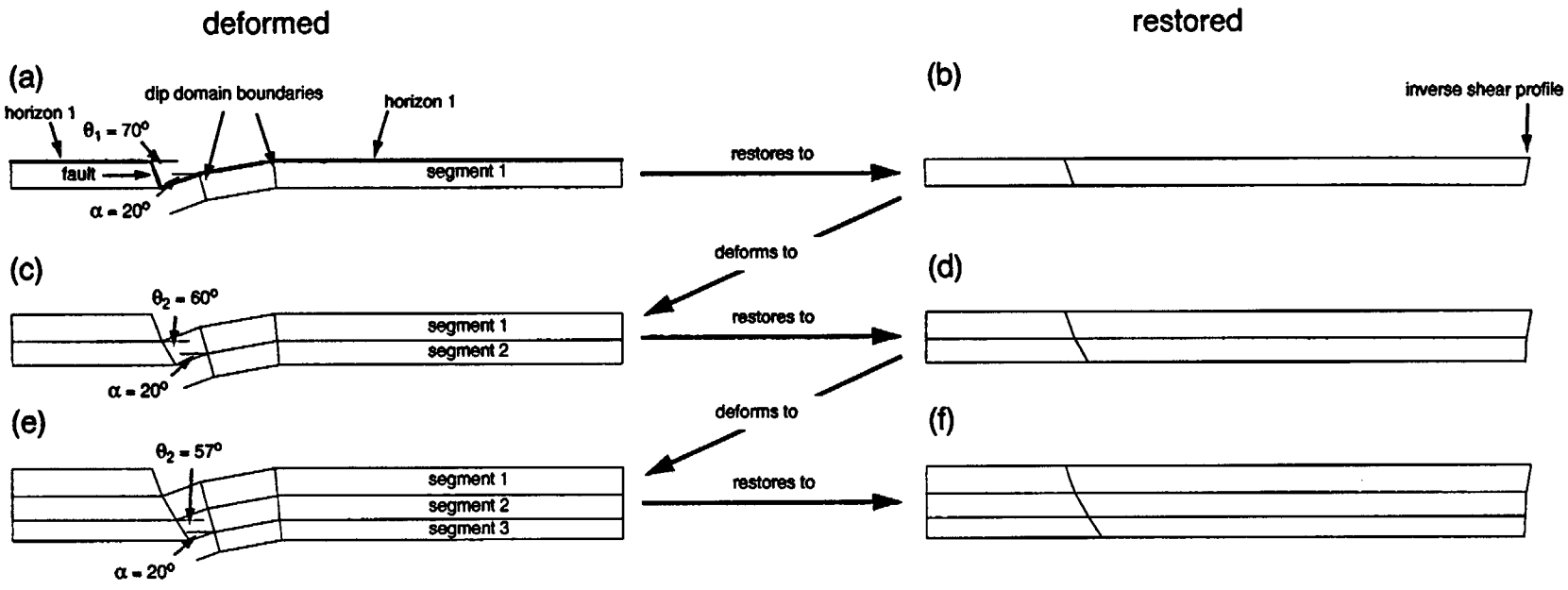

Morris and Ferrill Fig. 8

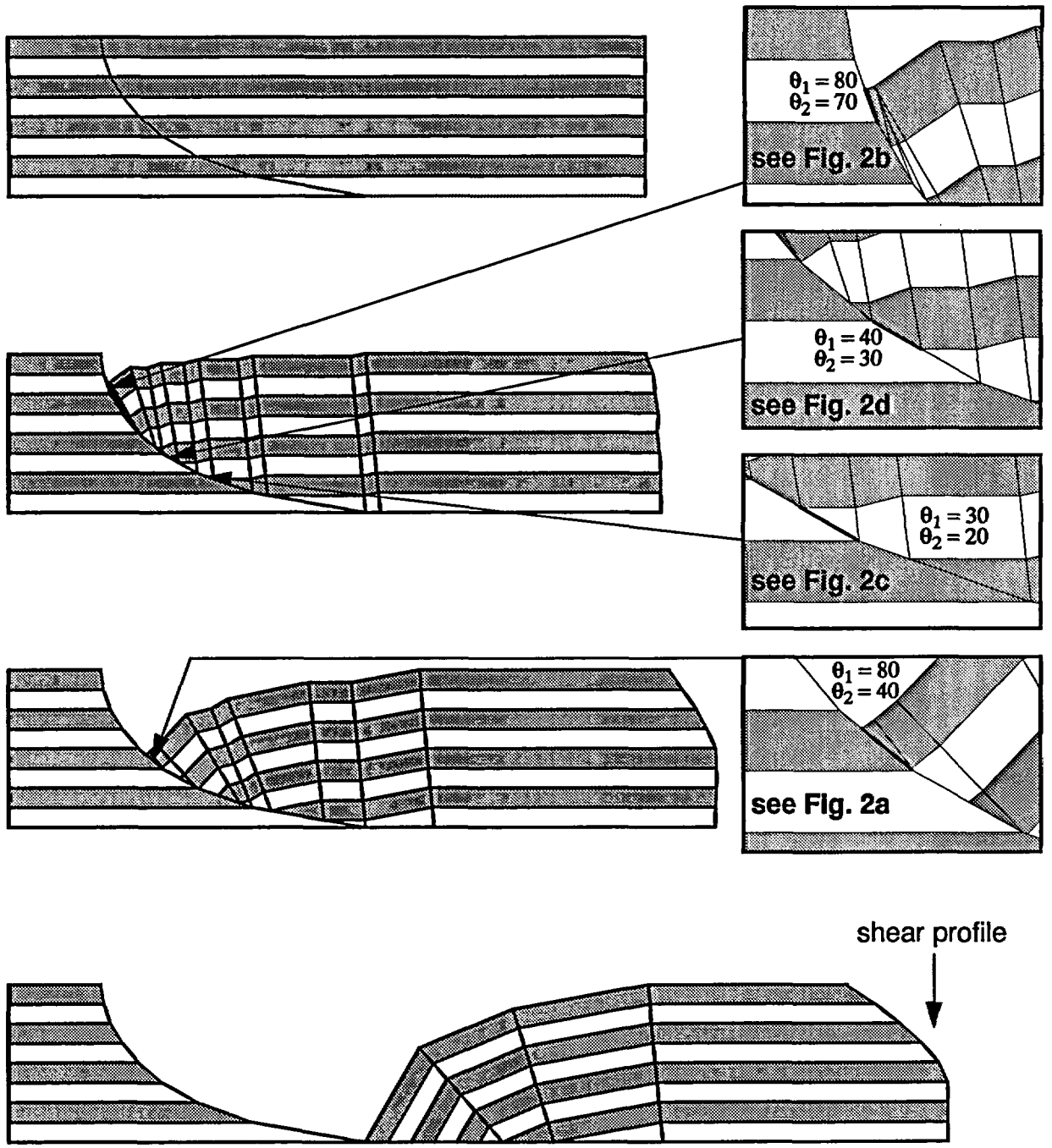

Morris and Ferrill Fig. 9

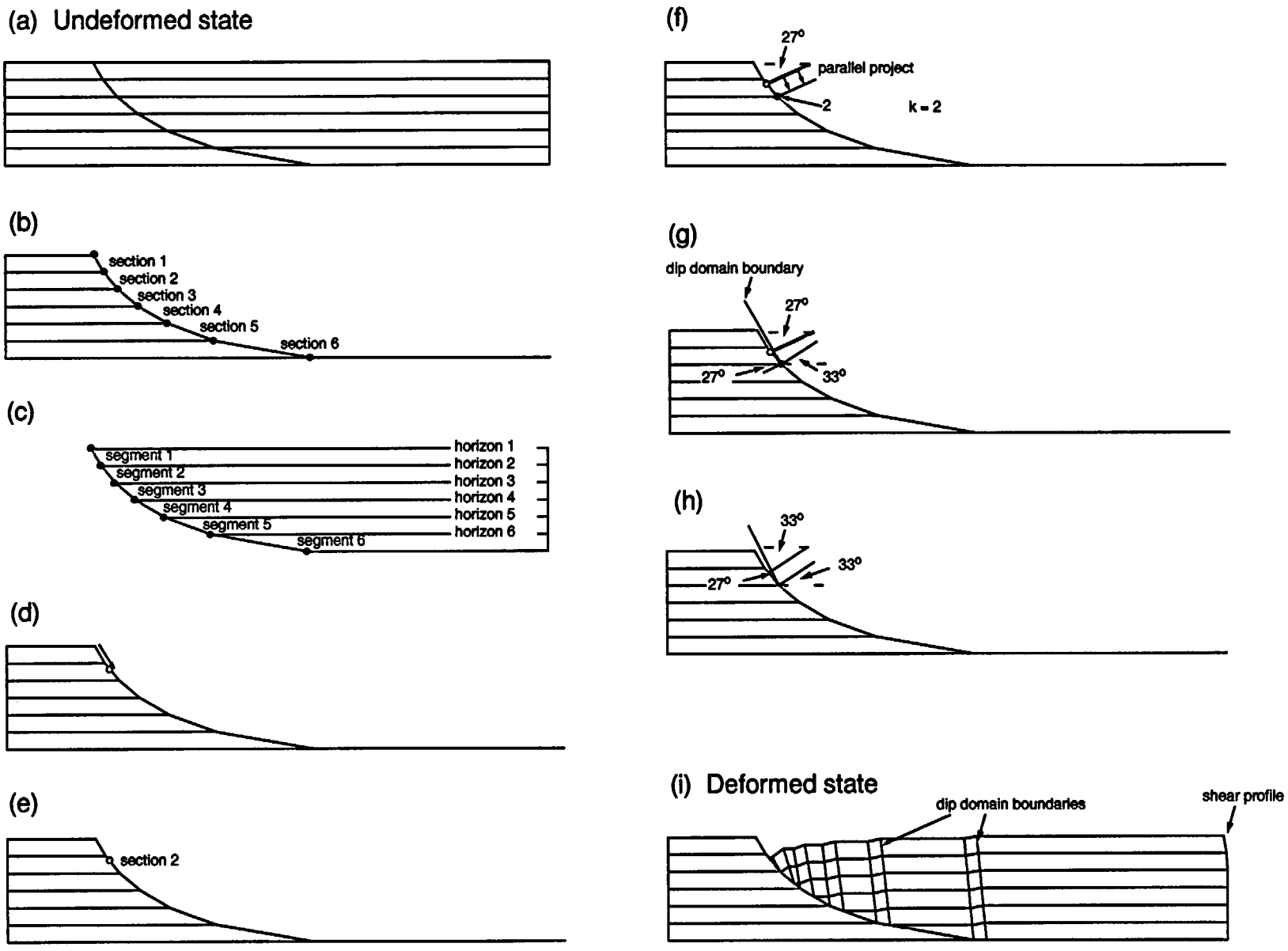

Morris and Ferrill Fig. 10